GO/ZnO nanocomposite-coated plastic optical fiber for copper ion detection in drinking water

NUR LIYANA ZAINOL[1], MUHAMMAD NIL YAFIQ MOHD YUSOF[1], WAN MAISARAH MUKHTAR[1], P. SUSTHITHA MENON[2], AFFA ROZANA ABDUL RASHID[1,*]
[1]*Faculty of Science and Technology, Universiti Sains Islam Malaysia, 71800, Nilai, Negeri Sembilan, Malaysia*
[2]*Institute of Microengineering and Nanoelectronics, Universiti Kebangsaan Malaysia, 43600 Bangi, Selang, Malaysia*

A plastic optical fiber (POF) sensor coated with graphene oxide (GO), zinc oxide (ZnO), and GO/ZnO nanocomposites was developed for the detection of copper ions (Cu^{2+}) in drinking water. The GO/ZnO nanocomposite was synthesized using a modified Hummer's method combined with solution mixing. The morphology, structure, and optical properties were characterized using FESEM, XRD, and UV-Vis spectroscopy. The POF was chemically etched and coated with the synthesized materials to enhance its sensitivity through evanescent wave interaction. Performance testing was carried out at copper ion concentrations of 0.7 ppm, 1.0 ppm, and 1.3 ppm, with optical power output measured using an optical power meter at 650 nm light source. Results demonstrated that GO-coated POF exhibited the highest sensitivity (0.0087 a.u/ppm) compared to ZnO and GO/ZnO-coated POFs. ZnO shows excellent linearity (99%), and the lowest limit of detection (0.2805 ppm), making it highly effective for detecting Cu^{2+} ions even at trace levels. This study highlights the potential of ZnO-coated POF sensors as a cost-effective, portable solution for heavy metal ion monitoring in water quality applications.

(Received October 18, 2025; accepted June 2, 2026)

Keywords: GO/ZnO nanocomposite, Plastic optical fiber, Copper ion detection

1. Introduction

Copper is an essential trace element for biological systems but becomes toxic when present in excessive concentrations in drinking water. The permissible limit set by the US Environmental Protection Agency (EPA) is 1.3 mg/L. Elevated Cu^{2+} levels, commonly caused by the corrosion of copper piping systems, can lead to gastrointestinal distress, liver damage, or kidney malfunction [1]. Reliable monitoring of copper ion concentration is therefore essential to ensure safe water quality. Conventional heavy metal detection techniques such as atomic absorption spectroscopy (AAS) and inductively coupled plasma mass spectrometry (ICP-MS) are accurate but are expensive, time-consuming, and require skilled personnel [2]. Optical fiber sensors present an alternative solution due to their portability, rapid response, and ability to operate in real-time [3]. Plastic optical fibers (POFs) are particularly advantageous compared to silica fibers because of their greater flexibility, higher elastic strain limit, lower cost, and ease of handling [4]. To utilize POFs for chemical and environmental sensing, a portion of the cladding is typically removed to expose the fiber core, allowing the evanescent field of the guided light to interact with the surrounding medium. The performance of these evanescent wave sensors depends significantly on the surface modification of the exposed core with functional nanomaterials. Therefore, selecting and engineering an optimal coating material is crucial for maximizing sensor sensitivity and selectivity.

Various materials have been explored for detecting heavy metal ions. For instance, chitosan, especially when combined with magnetic nanoparticles as nano-adsorbents, is effective for capturing and extracting these toxic ions [5]. Carbon nanoparticles particularly carbon nanotubes produce a distinct electrochemical response when integrated onto electrode surfaces enabling sensitive detection [6]. Additionally, gold nanoparticles offer advantages due to their antioxidant properties and high chemical stability [7], while titanium oxide with high surface area and photocatalytic properties enables detection of trace ions [8]. Nanomaterials such as graphene oxide (GO) and zinc oxide (ZnO) have attracted significant attention for their unique optical and electronic properties. GO provides abundant oxygen-containing functional groups that act as active binding sites for Cu^{2+} ions via electrostatic interactions, coordination bonds, and π-π interactions which potentially altering the electrical or optical properties of the GO [9]. Meanwhile, ZnO exhibits remarkable transparency, high electron mobility, a substantial exciton binding energy (60 meV), a wide band gap (3.37 eV) and strong luminescence at room temperature. A large exciton binding energy enables the material to generate excitons (electron-hole pairs) even at room temperature, which can participate in sensing reactions and increase the sensitivity of detection methods [10]. Combining GO and ZnO into a nanocomposite can synergistically enhance sensing performance by increasing surface area and active sites for interaction with analytes [11]. This study focuses on synthesizing GO/ZnO nanocomposites, characterizing their structural and optical

properties, and fabricating coated POF sensors for Cu^{2+} detection. The performance of GO, ZnO, and GO/ZnO-coated POF sensors is evaluated and compared to identify the most effective configuration for real-time copper ion monitoring.

2. Materials and methods

2.1. Synthesis of GO and GO/ZnO Nanocomposite

GO was synthesized using the modified Hummer's method where graphite powder and sodium nitrate ($NaNO_3$) were mixed with concentrated sulfuric acid (H_2SO_4) and kept in a freezer to maintain a low temperature before adding potassium permanganate ($KMnO_4$) as the oxidizing agent. The reaction mixture was gradually warmed to 35 °C while stirring until the color changed from green (Fig. 1(a)) to brown, indicating oxidation of graphite to graphite oxide. Upon the slow addition of distilled water, the color of the solution transitioned from dark brown at the base to a reddish-purple near the surface. Additionally, a visible purple gas was released into the air as shown in Fig. 1(b) which was likely due to the decomposition of manganese compound. The reaction was stopped by the careful addition of distilled water, followed by hydrogen peroxide (H_2O_2) to remove residual manganese ions, producing a yellow-brown suspension as shown in Fig. 1(c). The resulting GO was filtered, repeatedly washed with diluted HCl and deionized water, centrifuged several times, and dried overnight in an oven at 60 °C.

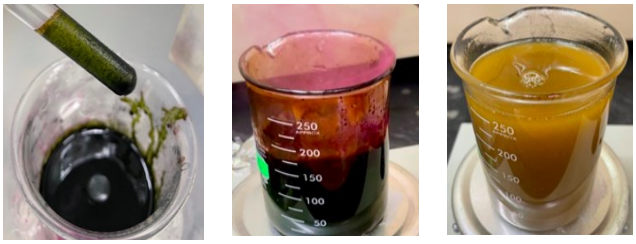

(a) (b) (c)

Fig. 1. Mixture turned to (a) dark green, (b)reddish-purple, (c)yellow-brown (colour online)

For the preparation of GO/ZnO nanocomposite, 0.12 g of ZnO powder was first dispersed in a 1:1 ethanol–water solution and sonicated for 2 hours to obtain a homogeneous ZnO dispersion. Simultaneously, a GO suspension was prepared by dispersing 0.12 g of dried GO in deionized water containing 1% SDS to prevent agglomeration. Equal volumes of ZnO dispersion and GO suspension were mixed and sonicated again for 30 minutes at ambient temperature. The pH of the mixture was adjusted to 10 using NaOH solution, and the mixture was heated in a water bath at 85 °C for 5 hours to promote nanocomposite formation. The resulting product was centrifuged, washed several times with deionized water to remove impurities, and finally dried at 50 °C to obtain GO/ZnO nanocomposite powder.

The crystalline structure was characterized using X-ray diffraction (XRD, Rigaku Miniflex 600) to provide critical insights into the extent of oxidation and structural modifications induced by the introduction of oxygen-containing functional groups into the synthesized GO via a modified Hummer's method. Surface morphology and particle dispersion were analyzed using field emission scanning electron microscopy (FESEM, Jeol) and UV-Vis spectroscopy (Varian Cary 50 Conc) was used to measure absorption spectra and estimate optical band gap energies of GO, ZnO, and GO/ZnO nanocomposite [12].

2.2. Fabrication of modified POF sensor

The fabrication of the POF sensor began by cutting a 30 cm long plastic optical fiber consisting of a 0.5 mm PMMA core and fluorinated polymer cladding. The protective jacket was carefully stripped at the central 5 cm section to expose the cladding layer. The unclad region was immersed in 60% acetone solution for chemical etching, then rinsed with deionized water. Fig. 2 displays the optical microscope image of (a) the unclad POF prior to etching process and (b) the etched POF. The etching process exposed the underlying core material, creating a rough texture that increases the surface area available for interaction with the surrounding medium. Then, the exposed fiber region was coated with three different materials which are GO, ZnO, and GO/ZnO nanocomposites using the dip-coating method

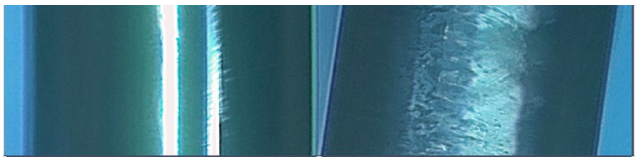

(a) (b)

Fig. 2. Microscope image of (a) unclad POF (b) etched POF (colour online)

For sensing measurements, copper sulfate pentahydrate stock solution was prepared and subsequently diluted to obtain Cu^{2+} solutions with concentration of 0.7 ppm, 1.0 ppm, and 1.3 ppm. The experimental setup consisted of a 650 nm LED light source coupled to one end of the coated POF, with an optical power meter attached to the opposite end as shown in Fig. 3. The coated region of the fiber was exposed to copper ion solutions, and the variations in transmitted optical power were recorded to evaluate the sensor's sensitivity, linearity, and repeatability.

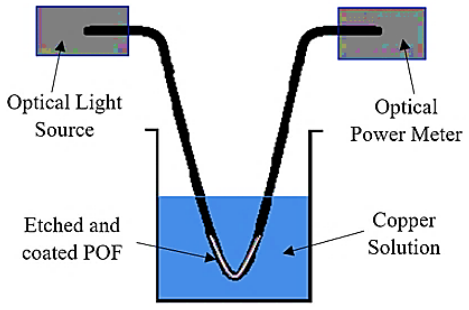

Fig. 3. Experimental setup of heavy metal ion detection (colour online)

2.3. Fiber optic sensor characterization

The sensitivity and performance of the sensor were evaluated by analyzing the interaction between the strong evanescent waves produced by the coated POFs and copper solution of various concentrations. The concepts of evanescent waves and penetration depth in optical fibers serves as the theoretical foundation for this testing methodology. When light propogates through an optical fiber, standing waves are formed due to total internal reflection at the core-cladding interface. The evanescent field of these standing waves penetrates into the fiber's cladding region to a specific depth, known as the penetration depth. The intensity of the evanescent field decays exponentially as the distance from the core and cladding interface increases. This exponential decay is described by equation (1).

$$I(d') = I_0 \cdot \exp(d_p - d') \quad (1)$$

where $I(d')$ is the intensity at a distance d' from the core, I_0 is the initial intensity of the input light and d_p is the penetration depth of the evanescent field.

In the context of the sensor testing, variations in optical transmission or absorbance result from the interaction between the sensor-generated evanescent waves and the copper analyte. The coated sensor exhibited high sensitivity towards different copper concentrations, with distinct changes in absorbance observed across concentrations of 0.7, 1.0 and 1.3 ppm. This variation in absorbance indicates the sensor's capacity to detect and respond to fluctuations in copper concentrations based on the interaction of the evanescent waves with the analyte. The sensitivity of the sensor was determined by plotting the power output ratio against the concentration of the copper solution, where the sensor sensitivity corresponds directly to the gradient value of the linear regression equation.

3. Results and discussion

3.1. Structural properties

The crystallinity of the synthesized samples was confirmed by X-ray diffraction (XRD) analysis illustrated in Fig. 4. The GO/ZnO nanocomposite exhibited distinct ZnO diffraction peaks at 2θ values of 31.844°, 34.506°, 36.332°, 47.616°, 56.657°, 62.916°, 68.004°, and 69.143°, corresponding to the (100), (002), (101), (102), (110), (103), (112), and (201) planes. Additionally, the presence of the (001) peak at 2θ ≈ 8.9° confirmed successful incorporation of GO into the ZnO matrix, forming a composite structure [13]. Slightly reduced peak intensity compared to pure ZnO suggests minor structural distortions due to GO integration, which can enhance surface activity for sensing applications [14]. The calculated crystallite size using the Scherrer equation of each peak ranging from 41 nm to 47.2 nm were summarized in Table 1.

Table 1. Summary of crystal structure parameter of GO/ZnO nanocomposite

Planes	2θ (°)	FWHM (°)	D (nm)
(001)	8.937	0.1540	41.175
(100)	31.844	0.1369	46.325
(002)	34.506	0.1333	47.560
(101)	36.332	0.1325	47.856
(102)	47.616	0.1294	49.003
(110)	56.657	0.1302	48.704
(103)	62.916	0.1293	49.036
(112)	68.004	0.1344	47.176
(201)	69.143	0.1369	46.327

The synthesized GO displayed two clear diffraction peaks at planes (001) and (002). A strong diffraction peak of graphite (002) was found at $2\theta = 27.44°$ with interlayer spacing distance (d-spacing) of 3.247 nm. This happened likely due to the existence of graphitic domains or partially reduced GO, which could result from incomplete oxidation or partial reduction during synthesis. If the oxidation process is not completely optimized, residual graphite may remain, resulting in the noticeable (002) peak. On the other hand, the (001) peak that shifted to the left was observed at at a lower angle $2\theta = 13.62°$. This confirmed the successful oxidation of graphite into GO, as it corresponds to increased interlayer spacing of 6.495 nm. The increased in interlayer spacing was due to the incorporation of oxygen functional groups such as hydroxyl and carboxyl as long as water molecules into the carbon layers [15].

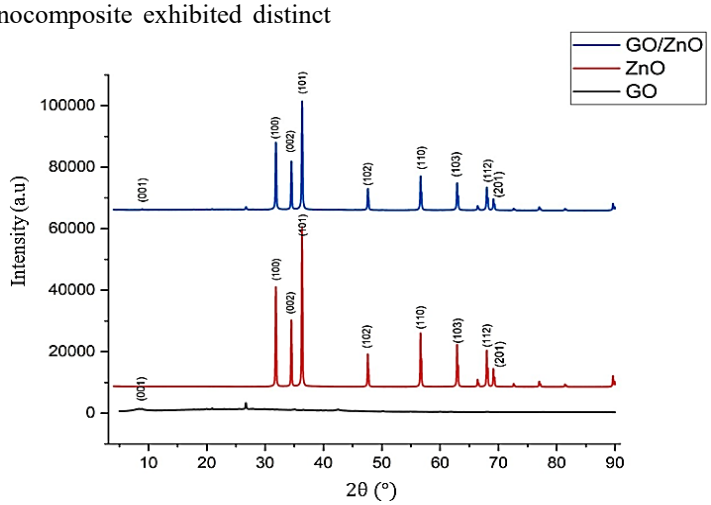

Fig. 4. XRD spectra of synthesized GO/ZnO nanocomposite (colour online)

3.2. Morphological properties

Fig. 5 (a) displayed the FESEM image of illustrated sheet-like structure indicative of graphene oxide. The observed sheet-like shape showed that GO was successfully synthesized utilizing the modified Hummers technique. These sheets appear to be interconnected, creating a network. In addition, the surface appeared rough and uneven, with creases and wrinkles on all surfaces. This roughness was most likely caused by the presence of oxygen-containing functional groups on the graphene oxide surface such as hydroxyl and epoxy groups [16]. The rough and uneven surface also validated the presence of oxygen-containing functional groups, which were introduced during the oxidation process. The ZnO particles exhibited a diverse morphology, ranging from rod-like structures to more irregular shapes, as shown in Fig. 5 (b). At 50 k magnification, the lengths of the rod-like structures were measured at 66.667 nm, 133.33 nm and 222.222 nm. Some agglomerates were also observed, where multiple particles were clustered together.

Fig. 5 (c) displays the FESEM image of GO/ZnO nanocomposite. As shown in the image, the irregularly shaped, rod-like ZnO nanoparticles were evenly distributed and integrated across the GO surface, forming agglomerations. This integration is attributed to the electrostatic attraction between the negatively charged GO and the positive Zn^{2+}ions [17]. In this nanocomposite, the length of rod-like structures increased compared to commercial ZnO, with measured lengths of 150 nm, 300 nm and 500 nm.

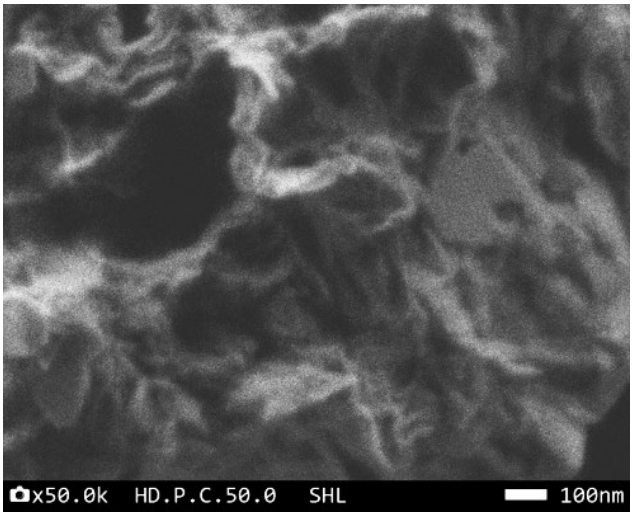

(a)

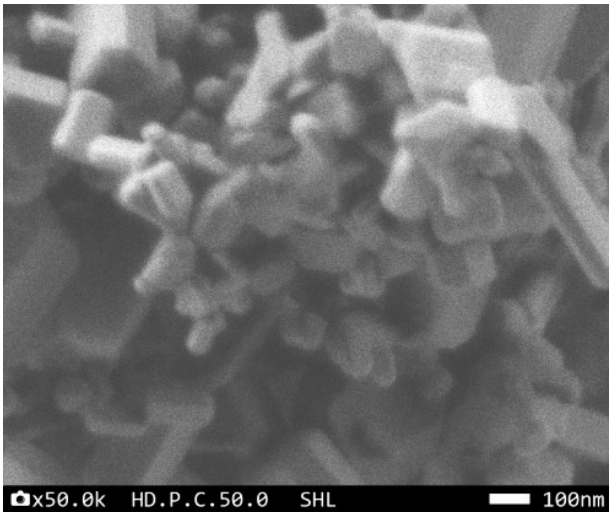

(b)

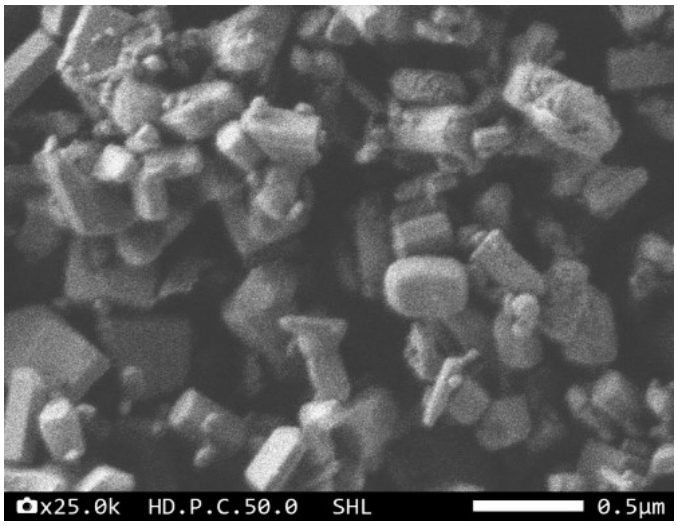

(c)

Fig. 5. FESEM images of (a) GO (b) ZnO (c) GO/ZnO

3.3. Optical properties

When GO was combined with ZnO, the resulting GO/ZnO nanocomposite exhibits unique optical properties that differ from those of the individual components. The interaction between GO and ZnO induced changes in the electronic structure and the material's band gap. The UV-Vis absorbance spectrum of GO, ZnO and GO/ZnO nanocomposite are shown in Fig. 6. The study indicates that the absorption spectrum of the GO/ZnO composite features increased absorbance in the UV-visible range compared to pure ZnO. This peak arises from the wide bandgap of ZnO (~3.28 eV), reflecting its strong ability to absorb UV light [18]. The absorbance gradually decreases at higher wavelengths, which is attributed to contributions from graphene oxide that typically exhibits broad absorption due to π–π* transitions. This mechanism was further verified by the fact that GO doping caused a rise in absorbance between 245 nm and 400 nm, indicating bandgap fluctuation in the nanostructured materials [13].

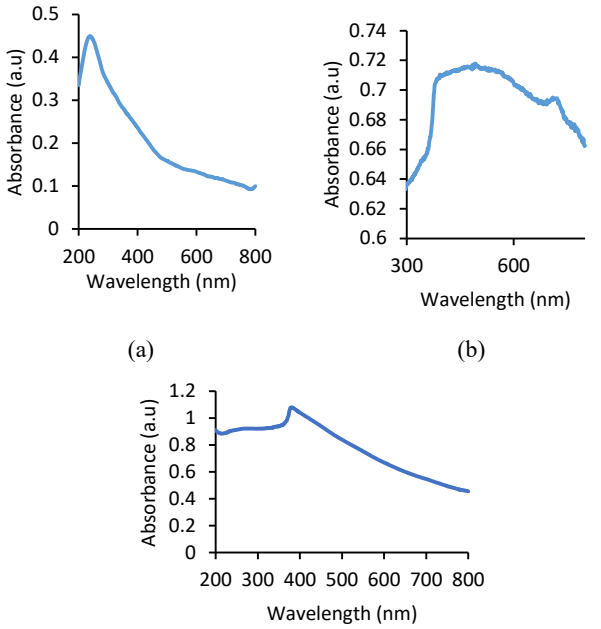

Fig. 6. The absorbance spectra of (a) GO, (b) ZnO, (c)GO/ZnO nanocomposite

Fig. 7 displayed the bandgap energy of synthesized GO/ZnO nanocomposite determined via Tauc plot analysis. The calculated bandgap of the nanocomposite is 3.32 eV, which is slightly higher than that of pure ZnO (3.28 eV) but lower than that of GO (3.74 eV). This broadening of the bandgap can be attributed to the integration of GO into the ZnO matrix. GO introduces modifications to the electronic structure, such as quantum confinement effects or alterations in the local electronic environment, which slightly widen the bandgap. This alteration has significant implications for the material's performance; a wider bandgap suggests enhanced UV absorption and reduced charge carrier recombination, thereby improving photocatalytic efficiency and optoelectronic performance. Furthermore, this shift indicates effective interaction and compatibility between GO and ZnO within the composite, leading to synergistic effects that enhance the material's properties beyond those of pristine ZnO [13].

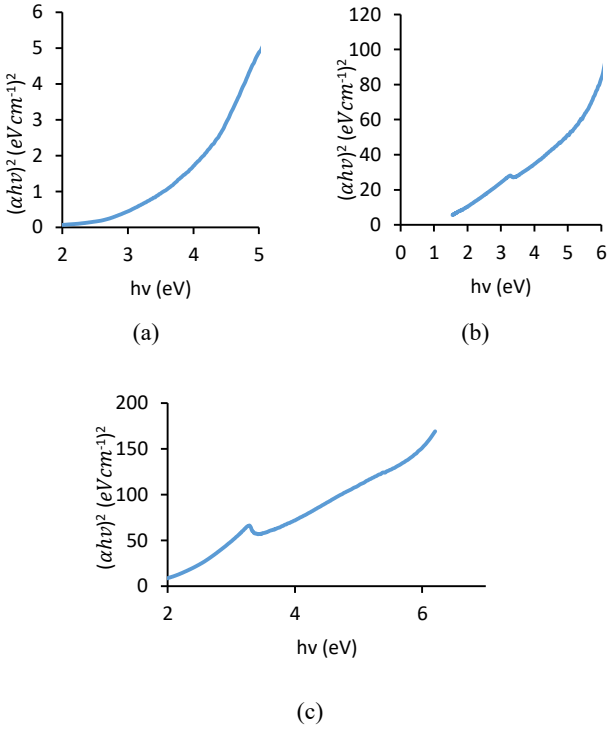

Fig. 7. Bandgap energy plot for of (a) GO, (b) ZnO, (c)GO/ZnO nanocomposite

Table 2. Summary of bandgap energy and refractive indices obtained for synthesized material

Material	Bandgap Energy (eV)	Refractive index (at 650 nm)
GO	3.74	1.08
ZnO	3.28	1.46
GO/ZnO	3.32	1.40

3.4. Sensor performance

Fig. 8 shows the sensitivity of uncoated and GO/ZnO-coated POF against concentration of copper ions. As shown in Fig. 8(a), the uncoated fiber displays a sensitivity of 0.0009 a.u/ppm with 85% linearity. Meanwhile, Fig. 8 (b) illustrates that the GO-coated POF performed better, exhibiting a sensitivity of 0.0087 a.u/ppm, which nearly ten times higher than that of the uncoated POF's with a linearity of 90%. Furthermore, the GO-coated POF achieved a lower LOD of 16.7102 ppm, indicating its ability to detect lower concentrations of copper ions compared to the uncoated POF, which had a much higher LOD of 58.0918 ppm. These results suggest that the incorporation of GO into the POF greatly enhanced

its sensitivity and detection capability [19]. The GO-coated POF displayed a gradual increase in optical power with increasing concentration, which is attributed to the progressive saturation of binding sites.

The performance of the ZnO-coated POF sensor, as shown in Fig. 8 (c) demonstrated a sensitivity of 0.0054 a.u/ppm with an excellent linearity of 99% and an LOD of 0.2805 ppm. This result indicated a superior capability for detecting low concentrations of copper ions compared to GO coated fiber. As illustrated in Fig. 8 (d), GO/ZnO-coated sensor exhibited a sensitivity of 0.0075 a.u/ppm with linearity of 95%, which was lower than GO-coated, but higher than ZnO-coated sensor. With LOD of 1.0961 ppm, the GO/ZnO sensor demonstrated greater efficacy than the GO-coated sensor in detecting lower concentrations of copper ions, yet it remained less effective than the ZnO-coated sensor (LOD of 0.2805 ppm). Table 3 summarizes the sensitivity, linearity, and limit of detection to compare the performance of each sensor.

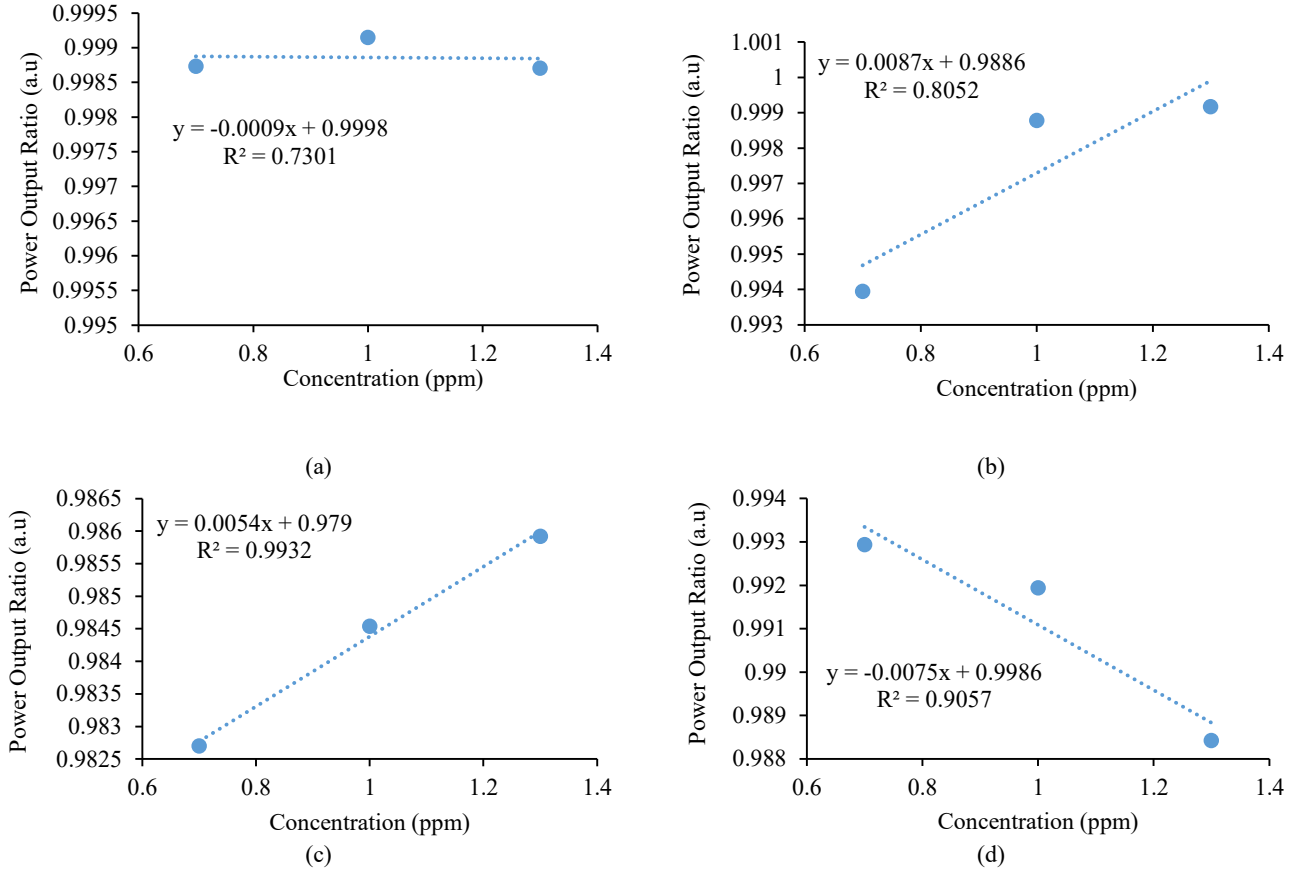

Fig. 8 Sensitivity of (a) uncoated (b) GO (c) ZnO and (d) GO/ZnO-coated POF against copper ions concentration

Table 3 highlighted that ZnO-coated POF exhibited the highest linearity and lowest LOD, making it highly effective for detecting Cu^{2+} ions even at trace levels. This can be attributed to ZnO's highly crystalline structure, confirmed by XRD, which provided numerous active sites for Cu^{2+} interaction and enhances detection accuracy [17]. The GO/ZnO-coated POF shows an optimal balance, with intermediate sensitivity and linearity between GO- and ZnO-coated POFs.

Table 3. Sensitivity, linearity and LOD of prepared samples

Modified POF sensor	Sensitivity (a.u/ppm)	Linearity (%)	LOD (ppm)
Bare	0.0009	85	58.0918
GO-coated	0.0087	90	16.7102
ZnO-coated	0.0054	99	0.2805
GO/ZnO-coated	0.0075	95	1.0961

4. Conclusion

In conclusion, GO-coated POF sensors exhibit the highest sensitivity among the tested coatings, whereas ZnO-coated fibers demonstrate superior linearity and the lowest limit of detection (LOD). Although GO provides the best sensitivity, its lower linearity limits its overall performance, as high sensitivity with poor linearity can result in inconsistent and unreliable measurements. Linearity is therefore often considered more critical than sensitivity for sensor reliability. The underlying optical fiber principle, where the core refractive index exceeds that of the cladding, enables total internal reflection and enhances evanescent wave interactions, improving the sensor's response. Moreover, ZnO's direct bandgap of 3.28 eV facilitates optimal optical and electronic behavior, further lowering the LOD and enhancing detection of small analyte changes, such as Cu^{2+} ions [20, 21]. The

GO/ZnO-coated POF achieves a balance between sensitivity and linearity, representing an optimal compromise between the properties of the individual materials. Overall, these findings highlight GO/ZnO as a promising coating for reliable, trace-level detection in optical fiber sensors.

Acknowledgements

The authors would like to thank Universiti Sains Islam Malaysia (USIM) for the resources and through grant scheme PPPI/USIM/FST/USIM/110823 provided.

References

[1] W. S. Hummers, R. E. Offeman, J. Am. Chem. Soc. **80**(6), 1339 (1958).
[2] D. R. Dreyer, S. Park, C. W. Bielawski, R. S. Ruoff, Chem. Soc. Rev. **39**(1), 228 (2010).
[3] M. Pesavento, A. Profumo, D. Merli, Sens. Actuators B Chem. **281**, 1 (2019).
[4] K. Peters, Smart Mater. Struct. **20**(1), 013002 (2010).
[5] Y. J. Beh, M. N. M. Nuzaihan, S. N. Sabki, S. B. Chia, C. H. Ng, C. C Ong, M. F. M. Fathil, Z. Zailan, International Journal of Nanoelectronics and Materials **16**(4), 827 (2024).
[6] S. F. Sulthana, U. M. Iqbal, S. B. Suseela, R. Anbazhagan, R. Chinthaginjala, D. Chitathuru, I. Ahmad, T. Kim, ACS Omega **9**(24), 25493 (2024).
[7] X. Xu, S. Yang, Y. Wang, K. Qian, Green Analytical Chemistry **2**, 100020 (2022).
[8] Y. Shi, S. Zhang, H. Zhou, Y. Dong, G. Liu, W. Ye, R. He, G. Zhao, Metals **15**(1), 80 (2025).
[9] C. Rodríguez, C. Tapia, E. Leiva-Aravena, E. Leiva, International Journal of Environmental Research and Public Health **17**(18), 6911 (2020).
[10] Md Ahmaruzzaman, S. Raha, Nanoscale Advances **4**, 1868 (2022).
[11] A. Pimentel, A. Gonçalves, D. Nunes, Materials Science in Semiconductor Processing **13**(2), 59 (2010).
[12] Y. Zhang, B. Zheng, Y. Zhu, H. Zhang, J. Hazard, Materials **387**, 121705 (2020).
[13] V. K. Gupta, S. Agarwal, T. A. Saleh, Environmental Science and Pollution Research **22**(1), 495 (2015).
[14] H. M. Yadav, S. V. Otari, S. D. Delekar, Journal of Environmental Chemical Engineering **8**(1), 103701 (2020).
[15] A. H. Surani, A. R. A. Rashid, N. Arshad, A. A. N. Hakim, International Journal of Nanoelectronics & Materials **12**(4), 0 (2019).
[16] B. Li, T. Liu, Y. Wang, Z. Wang, Journal of Colloid Interface Science **377**(1), 114 (2012).
[17] Q. Liu, Y. Zhou, Z. Li, J. Mater. Sci. **54**, 588 (2019).
[18] D. Xie, H. Zhang, G. Wang, L. Xue, X. Yang, W. Shi, J. Yao, Results in Physics **29**, 104707 (2021).
[19] A. R. A. Rashid, A. H. Surani, W. M. Mukhtar, N. Arsad, P. S. Menon, Optoelectron. Adv. Mat. **18**(5-6), 217 (2024).
[20] M. Pesavento, A. Profumo, D. Merli, L. Cucca, L. Zeni, N. Cennamo, Sensors **19**(23), 5246 (2019).
[21] Ü. Özgür, M. Yaşar, F. Atay, Journal of Materials Science: Materials in Electronics **30**(11), 10134 (2019).

*Corresponding author: affarozana@usim.edu.my